PHYSICO-CHEMICAL PRINCIPLES
OF MATERIALS DEVELOPMENT

Dislocation Sinks Efficiency for Self-Point Defects in Iron and Vanadium Crystals

A. B. Sivak[a, b]**, P. A. Sivak**[a]**, V. A. Romanov**[b, c]**, and V. M. Chernov**[b, d]

[a]*National Research Centre "Kurchatov Institute," Moscow, Russia*
[b]*Tomsk State University, Tomsk, Russia*
[c]*State Research Center of the Russian Federation, Institute for Physics and Power Engineering, Obninsk, Russia*
[d]*Bochvar National Research Institute for Inorganic Materials, Moscow, Russia*
e-mail: sivak_ab@nrcki.ru, sivak_pa@nrcki.ru, romanov-ippe@mail.ru, chernovv@bochvar.ru
Received June 2, 2014

Abstract—The effect of the dislocations stress fields on their sink efficiency for self-point defects (interstitial atoms and vacancies) is studied in the temperature range of 293−1000 K and at the dislocation density values of $1 \times 10^{12}−3 \times 10^{14}$ m^{-2} in body-centered cubic (BCC) iron and vanadium crystals. Straight screw and edge dislocations in $\langle 111 \rangle \{110\}$, $\langle 111 \rangle \{112\}$, $\langle 100 \rangle \{100\}$, and $\langle 100 \rangle \{110\}$ slip systems are considered. Defect diffusion is simulated via the object kinetic Monte Carlo method. The energies of the interaction of defects with dislocations are calculated within the anisotropic linear theory of elasticity. The dislocation sink efficiency is analytically represented as a function of temperature and dislocation density.

Keywords: iron, vanadium, vacancies, self-interstitial atoms, diffusion, dislocation sink efficiency, object kinetic Monte Carlo method

DOI: 10.1134/S2075113315020161

INTRODUCTION

Basic radiation microstructural modifications in metals are defined by the formation and diffusion of point defects in them, as well as by the reactions between these defects and with dislocations [1−4]. The kinetics of such processes depends considerably on the elastic stress fields (internal and external). The dislocations are the main sources of internal stresses in crystals, and the fields of such stresses significantly affect the kinetics of the self-point defects (SPDs—the self interstitial atom (SIA) and the vacancy), including their diffusion and absorption by the dislocation cores as the SPDs sinks. These processes depending on the crystal symmetry, elastic anisotropy of crystals, and defect types [1−7] define the behavior of the microstructure and properties of crystals under external influences of different nature (mechanical, thermal, and radiation).

The efficiency of dislocation sinks (DSs) is determined by the magnitude $\xi = k^2/\rho_d$, where k^2 is the sink strength (k^{-1} is the diffusion length for the SPD before absorption by a sink) and ρ_d is the dislocation density [8]. Taking into account the interaction between sinks (stress sources) and SPDs is important when determining the DS efficiency, since the SPD configurations (stable and saddle) exhibit different point symmetry on the diffusion paths to the sinks. The DS efficiency should not be calculated (or estimated) by means of isotropic approximations (the isotropic the-

ory of elasticity and the spherical symmetry of all defect configurations [2, 9]) or defined a priori [8, 10−12], since such approximations lead to the disappearance of qualitative differences between crystals of various crystallographic classes and types of dislocations and point defects (elastic dipoles). Metals belong to elastic anisotropic crystals with the parameter of elastic anisotropy (for a cubic crystal system)

$$A_{el} = \frac{2C_{44}}{C_{11}-C_{12}},$$

where C_{11}, C_{12}, and C_{44} are the elastic constants. For the BCC metals with a few exceptions, the parameter A_{el} is different from one (in the isotropic case, $A_{el} = 1$). At room temperature for iron, $A_{el} = 2.36$; for vanadium, $A_{el} = 0.78$ [13].

This work is aimed at exploring the effect of the stress fields of the dislocations on their sink efficiency for SPDs over the temperature range of 293−1000 K and in the dislocation density range of $1 \times 10^{12}−3 \times 10^{14}$ m^{-2} in Fe and V BCC crystals, which are the basis of promising steels and alloys for nuclear and thermonuclear reactors.

COMPUTATIONAL METHODS
AND PARAMETERS

Straight screw and edge dislocations (SDs and EDs, respectively) in $\langle 111 \rangle \{110\}$, $\langle 111 \rangle \{112\}$,

Table 1. Burgers vector **b**, normal to the slip plane **n**, and direction **t** of the considered straight edge (ED) and screw (SD) dislocations

Dislocations	**b**	**n**	**t**
ED⟨111⟩{110}	1/2 [111]	[$\bar{1}$10]	[11$\bar{2}$]
ED⟨111⟩{112}	1/2 [111]	[11$\bar{2}$]	[$\bar{1}$10]
ED⟨100⟩{100}	[100]	[001]	[010]
ED⟨100⟩{110}	[100]	[011]	[01$\bar{1}$]
SD⟨111⟩	1/2 [111]	[$\bar{1}$10]	[111]
SD⟨100⟩	[100]	[001]	[100]

⟨100⟩{100}, and ⟨100⟩{110} slip systems have been considered. SPDs diffusion in elastic fields was simulated via the object kinetic Monte Carlo (OKMC) method [14, 15]. The energy of the elastic interaction of SPDs (elastic dipoles) in stable and saddle positions with dislocations was calculated within the anisotropic linear theory of elasticity (ALTE) [13].

For comparison, the linear sink efficiency for diffusing SPDs which do not interact with the sinks and are absorbed by the sinks in contact with the cores and having a certain radius of absorption (noninteracting linear sinks—NILSs) will also be calculated. The directions, densities, and radius of absorption of NILSs are in agreement with the dislocation sinks (DSs) interacting with SPDs. The values of SPD dipole tensors needed for the calculations were obtained in [6, 16−18] via the molecular static method. The crystallographic (right) coordinate system will be used throughout the paper.

The SPD formation energy E_d^F in crystals with dislocations is determined as

$$E_d^F = E^F + E^{int}(\mathbf{r}), \qquad (1)$$

where E^F is the SPD formation energy in the absence of dislocations; $E^{int}(\mathbf{r})$ is the interaction energy of SPD with the dislocation, and $\mathbf{r}$ is the radius vector of SPD position relative to the center of the dislocation core. The energy E^{int} within the ALTE (size interaction) has the form [5, 13, 19]

$$E^{int}(\mathbf{r}) = -P_{ij}\varepsilon_{ij}(\mathbf{r}), \qquad (2)$$

where ε_{ij} is the elastic deformation tensor induced by a dislocation and P_{ij} is the SPD dipole tensor; here, summation is implied over repeated indices ($i, j = 1, 2, 3$).

In Fe and V BCC crystals, the ⟨110⟩ dumbbell configuration [16] has the minimum formation energy in the absence of stress fields among various SIA configurations, which will further be considered as the initial one. Two mechanisms of SPD migration will be considered: a jump of the ⟨110⟩ SIA dumbbell configuration into the nearest neighbor lattice site with the dumbbell axis rotation by 60° and a jump of a vacancy into the nearest neighbor site.

The elastic constants C_{11}, C_{12}, and C_{44} and the lattice parameter a used for calculating the elastic dislocation fields correspond to the magnitudes provided by the interatomic interaction potentials [17, 18], and are reported in [6, 16−18]. The crystallographic characteristics and designations of the considered dislocations are shown in Table 1.

The DS efficiency was evaluated via the OKMC method [7, 16]. In this case, it is assumed that a model crystal has only a single SPD and a single sink type (the given dislocation type). The initial SPD positions were randomly assigned through the crystallite. The model crystallite was a prism with unlimited length and a square with a side length L lying in its base. The dislocation was at the center of the prism. Periodic boundary conditions were imposed on the side faces of a prism: if an SPD leaves the crystallite, it returns back from the opposite crystallite side. A crystal with a square network of parallel dislocations with the distances between the nearest dislocations $L(\rho_d = L^{-2})$ was thus simulated. The SPD trajectory was calculated until the SPD was absorbed by the dislocation (approached the dislocation at a distance smaller than some critical value r_0). After that, a new SPD of the same type was introduced into the model crystallite. The sink efficiency is determined as follows:

$$\xi = \frac{k^2}{\rho_d} = \frac{2dL^2}{l^2\langle N \rangle}, \qquad (3)$$

where $l = 3^{1/2}a/2$ is the SPD jump length in the BCC lattice, $\langle N \rangle$ is the average number of SPD leaps until the absorption by the sink, and $d = 3$ is the dimensionality of motion. For acquiring statistically reliable data, at least 10^5 trajectories were simulated for each dislocation type and SPD, which ensured the calculation error of ξ at a level below 1% (the confidence probability is assumed to be 99%). In some cases, up to 10^7 trajectories were calculated, which increased the accuracy of the calculation by an order of magnitude (with the error below 0.1%).

In the present work for Fe and V BCC crystals, the absorption radius is assumed to be equal to $r_0 = 3a$. Some uncertainty of the criterion for choosing r_0 magnitude exerts no significant influence on the calculated DS efficiency values, since the field interaction between SPDs and dislocations makes the determining contribution to the magnitude of ξ. Figure 1 displays the difference in DS efficiencies with the absorption radii of $r_0 = 3a$ and $r_0 = a$ as functions of DS efficiency with the absorption radii of $r_0 = 3a$ in Fe and V at $\rho_d = 3 \times 10^{14}$ m^{-2} for different dislocation types, SPDs, and temperatures. This difference decreases exponentially with the growth in DS efficiency (approximation of the calculated data):

$$1 - \left[\frac{\xi(r_0 = a)}{\xi(r_0 = 3a)}\right] = 10^3 \exp[-4\xi(r_0 = 3a)]. \quad (4)$$

The calculated DS efficiencies for $r_0 = 3a$ and $r_0 = a$ coinside in the limits of statistical uncertainty of the calculations at $\xi(r_0 = 3a) > 3$ (Fig. 1). The use of the ALTE for the calculation of the size interaction of the dislocation with SPD at a distance between them below $3a$ leads to a noticeable underestimate of the total energy of interaction [7], because other types of interaction (short-range ones like module interaction, etc. [20]) are not taken into account, while their consideration could reduce the difference in magnitude of ξ for $r_0 = 3a$ and $r_0 = a$. In the limiting case of absence of interaction between SPD and dislocation (NILS), the decrease in the magnitude of r_0 by a factor of 3 leads to the decrease in the NILS efficiency ξ_0 by 28% at a maximum dislocation density of 3×10^{14} m^{-2} taken in this paper—at smaller dislocation densities, the change in ξ_0 would be less.

The interaction energy E^{int} (2) depends on the temperature because of the temperature dependence of the P_{ij} and ε_{ij} tensors.

The change in components P_{ij} with temperature can be estimated by means of molecular dynamics (MD). The relaxation volume V^R and the trace of the dipole tensor TrP_{ij} for SPD are related by the ratio [21]

$$V^R = \frac{\text{Tr}P_{ij}}{3K}, \quad (5)$$

where $K = (C_{11} + 2C_{12})/3$ is the bulk modulus. As follows from the bulk modulus definition ($K = -Vdp/dV$, where p is the pressure and V is the volume), the additionally created SPD in the equilibrium model crystallite with a constant volume V (periodic boundary conditions) induces the pressure

$$p = \frac{KV^R}{V} = \frac{\text{Tr}P_{ij}}{3V} \quad (6)$$

in the crystallite. The MD calculations revealed that, with the increase in temperature from room to 1000 K, the change in the pressure within the crystallite and thus in the dipole tensor trace in accordance with (6) is below 15% for the $\langle 110 \rangle$ dumbbell configuration of SIA and vacancy. The OKMC calculations revealed a change in ξ values for Fe and V crystals at 1000 K no greater than 10% at a proportional decrease in all dipole tensor components of 15%.

The elastic strain field of a dislocation ε_{ij} depends on certain combinations of elastic constants rather than on their values [13]. For example, the parameters A_{el} and $B_{el} = C_{44}/K$ can be chosen as such a set of combinations. In V crystal with increasing temperature from 0 to 1000 K the value of A_{el} changes by 8% (from 0.81 to 0.75), and the value of B_{el} changes by 16% (from 0.29 to 0.25) [22]. In Fe crystal with increasing temperature from 0 to 1000 K, the changes in the values of A_{el} and B_{el} are, respectively, 96% (from 2.3 to 4.5) and 9% (from 0.70 to 0.77) [22]. In accordance
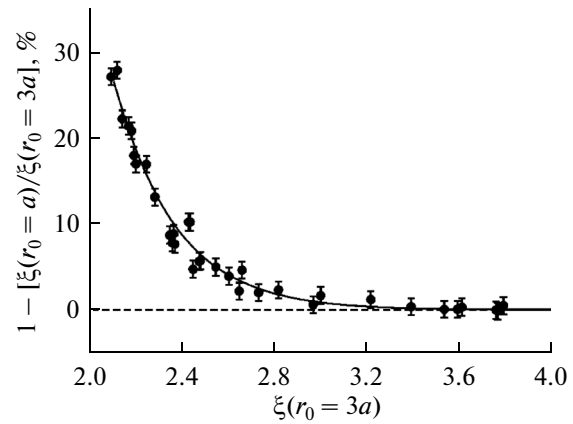

Fig. 1. Difference in DS efficiencies ξ with the absorption radii $r_0 = 3a$ and $r_0 = a$ at the dislocation density of 3×10^{14} m^{-2} for different materials (Fe and V), dislocation types, SPDs, and temperatures. The points are the OKMC data with indicated statistical error. The solid line is the approximation of OKMC data.

with the OKMC calculations, the change in the values of ξ for different dislocation types in Fe at 1000 K is no greater than 10% with change in the values of elastic constants in the temperature range of 0 to 1000 K.

Since the change in values of P_{ij} and ε_{ij} with temperature weakly affects the value of ξ in the considered temperature range of 293–1000 K, the temperature impact on values of P_{ij} and ε_{ij} was not taken into account in a further calculation of E^{int}.

RESULTS AND DISCUSSION

Noninteracting Linear Sinks (NILSs)

The efficiency of NILSs is defined by many factors such as their density, absorption radius, spatial distribution, and SPD type. Nevertheless, some of these factors can be neglected; namely, we assume that the NILS efficiency does not depend on NILS spatial distribution and SPD type. In addition, since the absorption radius in the present work was assumed to be $3a$, there is no need for taking into consideration the effect of its value on the NILS efficiency. The calculated impact of the factors listed above is given in Appendix A.

The present work needs the functional dependence of the NILS efficiency on the dislocation density. Solving the diffusion equation gives the following expression for the NILS efficiency [23, 24]:

$$\xi_{0,th}(\rho) = \frac{2\pi}{\ln\left(\frac{1}{\rho}\right) - \frac{3}{4}}, \quad (7)$$

where $\rho = r_0 (\pi\rho_d)^{1/2}$, and the terms ρ^2 and ρ^4 are not given, since the maximum magnitude of ρ used in this paper takes the value $0.015\pi^{1/2}$. Expression (7) does not take into account that SPDs perform jumps of the

Table 2. DS efficiency $\xi^{\pm}$ ("+" for SIA and "−" for vacancies) at 293 K and dislocation density of 3×10^{14} m^{-2} in Fe and V BCC crystals. The error is below 0.1%

Dislocations	ξ^{+} (Fe; V)	ξ^{-} (Fe; V)
ED⟨111⟩{110}	8.545; 5.734	2.951; 3.605
ED⟨111⟩{112}	8.730; 5.714	2.978; 3.587
ED⟨100⟩{100}	8.501; 5.959	2.652; 3.528
ED⟨100⟩{110}	9.674; 6.081	2.992; 3.695
SD⟨111⟩	3.761; 2.891	2.237; 2.085
SD⟨100⟩	4.491; 3.443	2.811; 2.540

finite length, which leads to the dependence of the NILS efficiency not only on the magnitude of ρ but also on r_0 [16]. Analysis of the OKMC calculations of the NILS efficiency for SPDs for various ρ and $r_0 = 3a$ enabled us to refine expression (7):

$$\xi_0(\rho) = \xi_{0,th}(\rho)(1 - 0.016\xi_{0,th}(\rho)). \quad (8)$$

Effect of Dislocation Type on the Dislocation Sink Efficiency

The calculated DS efficiencies for SIA and vacancies (ξ^{+} and ξ^{-}, respectively) for dislocations in different slip systems at temperature $T = 293$ K and $\rho_d = 3 \times 10^{14}$ m^{-2} ($L = 200a$) in Fe and V BCC crystals are shown in Table 2.

Analysis of ratio (2) reveals the following in BCC crystals:

(i) The interaction of SDs with the saddle point configurations of vacancies and SIAs is mainly determined by off-diagonal components P_{ij}.

(ii) The interaction of EDs with the saddle point configurations of vacancies and SIAs is determined by both off-diagonal and diagonal components P_{ij}.

The values of ξ^{+} are higher in Fe than in V because of the higher values of components P_{ij} of the saddle point SIA configuration in Fe than in V. The values of ξ^{+} are much higher for EDs than for SDs, since the values of the diagonal components P_{ij} of the saddle point SIA configuration are superior to the values of the off-diagonal components.

For EDs, the values of ξ^{-} in Fe are lower than in V, since the values of the diagonal components P_{ij} for the vacancies in Fe are much lower than the relevant values in V. For SD, the off-diagonal components P_{ij} for the saddle point vacancy configurations play the key role in the interaction with vacancies. Because the values of the mentioned components are higher in Fe than in V, the values of ξ^{-} in Fe are correspondingly superior to those in V.

In V, the values of ξ^{-} are much higher for EDs than for SDs, since the values of the diagonal components P_{ij} for the saddle point vacancy configurations are superior to the values of the off-diagonal components.

In Fe, the values of the diagonal and off-diagonal components P_{ij} for the saddle point vacancy configurations are almost equal, and therefore the values of ξ^{-} for EDs and SDs are close to each other.

For all the above dislocations, the relation $\xi^{+} > \xi^{-}$ is satisfied, since the components P_{ij} of the saddle point SIA configuration exhibit higher absolute values compared to the relevant values for the vacancies.

The spread of values of $\xi^{\pm}$ for EDs relative to the mean value over all considered EDs does not exceed 9% and 4% for Fe and V, respectively (Table 2). The similar distribution for SDs is below 12% and 10% for Fe and V, respectively (Table 2).

The dislocations field has a strong angular dependence [13], which results in a spatial inhomogeneity of the SPDs trajectories distribution. As an example, Fig. 2 displays the angular distributions of the SPDs absorbed by ED⟨111⟩{110}, ED⟨100⟩{100}, SD⟨111⟩, and SD⟨100⟩ dislocations at $T = 600$ K and $\rho_d = 3 \times 10^{14}$ m^{-2} in Fe (the angles are calculated counterclockwise from the slip plane of the dislocation (Table 1) in the plane perpendicular to the dislocation line). The change in ρ_d exerts almost no influence on the angular absorption distribution.

Most SIAs are absorbed by the edge dislocations in the range of angles from 0° to 180°; for vacancies, from 180° to 360° (Figs. 2a, 2b). The above features of the SPD absorption by the ED⟨111⟩{110} and ED⟨100⟩{100} edge dislocations are retained also for ED⟨111⟩{112} and ED⟨100⟩{110} dislocations.

The maximum fractions of SIA absorbed by SD⟨111⟩ dislocations are in the range of angles near 30°, 150°, and 270°; for vacancies, 90°, 210°, and 330° (Fig. 2c). The maximum fractions of SIAs absorbed by SD⟨100⟩ dislocations are in the range of angles near 0°, 90°, 180°, and 270° (Fig. 2d).

Temperature Impact on the Dislocation Sink Efficiency

To clarify the temperature dependence of the DS efficiency $\xi(T)$, the calculations were implemented for the edge and screw dislocations in the ⟨111⟩{110}, ⟨111⟩{112}, ⟨100⟩{100}, and ⟨100⟩{110} slip systems at temperatures of 293, 400, 600, 800, and 1000 K and $\rho_d = 3 \times 10^{14}$ m^{-2} ($L = 200a$) in Fe and V crystals (Fig. 3).

The calculated dependences $\xi(T)$ are well described by the equation

$$\xi(T) = \xi_0 \left[1 + AT^{-1} \exp\left(-\frac{T}{B}\right) \right], \quad (9)$$

where A and B are fitting parameters (Table 3) and ξ_0 is the NILS efficiency (8). It is seen from Fig. 3 that these dependences describe the OKMC data well over the considered temperature range. In Fig. 3, the solid lines indicate the NILS values. The parameters A and B are correlated with each other, and their relationship is discussed in Appendix B.
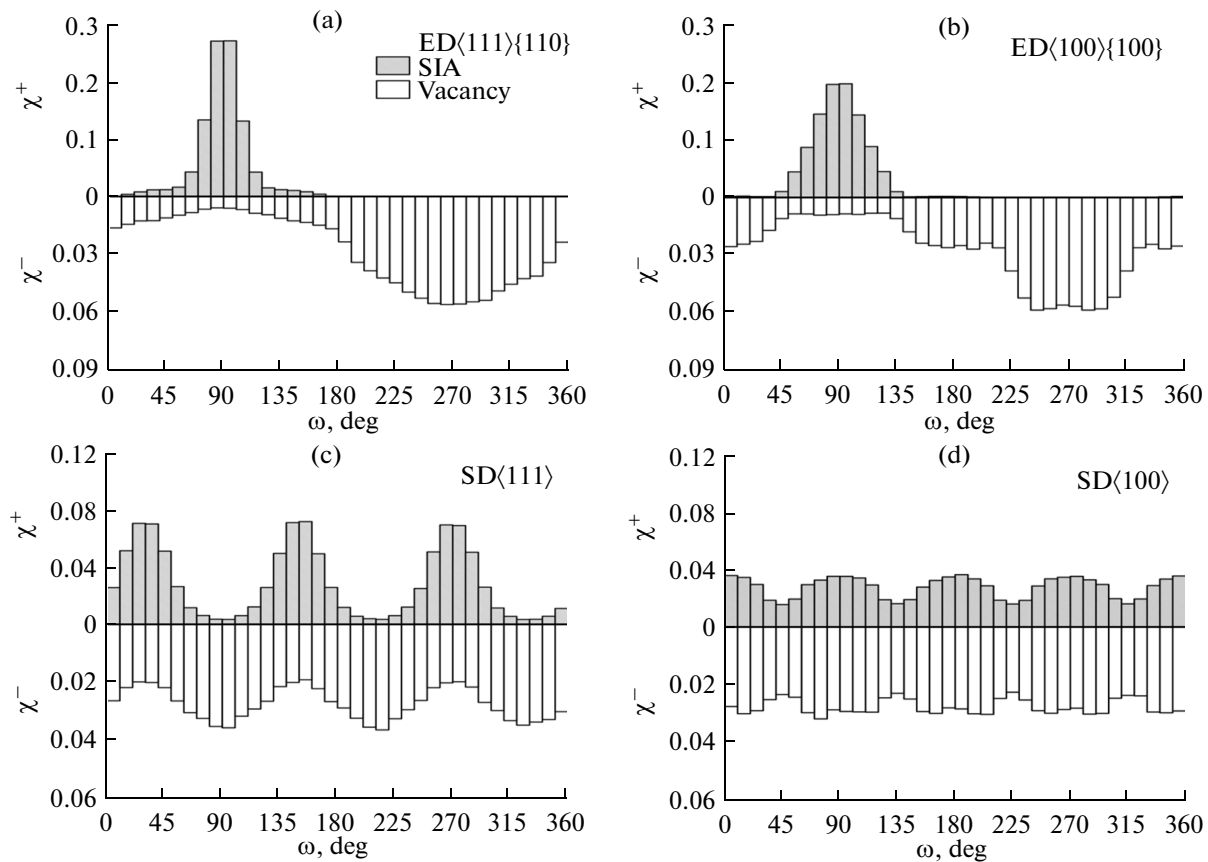
Fig. 2. Angular distributions of the fraction of SIAs (χ^+) and vacancies (χ^-) absorbed by the dislocations: (a) ED$\langle 111 \rangle \{110\}$, (b) ED$\langle 100 \rangle \{100\}$, (c) SD$\langle 111 \rangle$, and (d) SD$\langle 100 \rangle$ at 600 K and the dislocation density of 3×10^{14} m^{-2} in Fe BCC crystal. The angle ω is calculated counterclockwise from the dislocation slip plane in the plane perpendicular to the dislocation line.

The DS efficiency decreases with the growth in temperature and in the limit tends to ξ_0. As a result, the difference in ξ^+ and ξ^- decreases with rising temperature. This difference can be characterized by the dislocation bias factor: $D = 1 - \xi^-/\xi^+$. Figure 4 depicts the dependences $D(T)$ for the same dislocations shown in Fig. 3.

As is evident from Fig. 4, the relation $\xi^+ > \xi^-$ ($D > 0$) is satisfied for all considered dislocations. At tempera-

tures above 600°C, the dislocation preference is much higher for the edge dislocations than for the screw ones.

Effect of the Dislocation Density on the Dislocation Sink Efficiency

Reconstruction of kinetic models requires the knowledge of the DS efficiency as a function of the value of ρ_d. For this purpose, the values of ξ were cal-

Table 3. Values of parameters $A^\pm$ and $B^\pm$ (in K, "+" for SIA and "−" for vacancies) in (9) for various types of dislocations in Fe and V BCC crystals with the dislocation density of 3×10^{14} m^{-2}

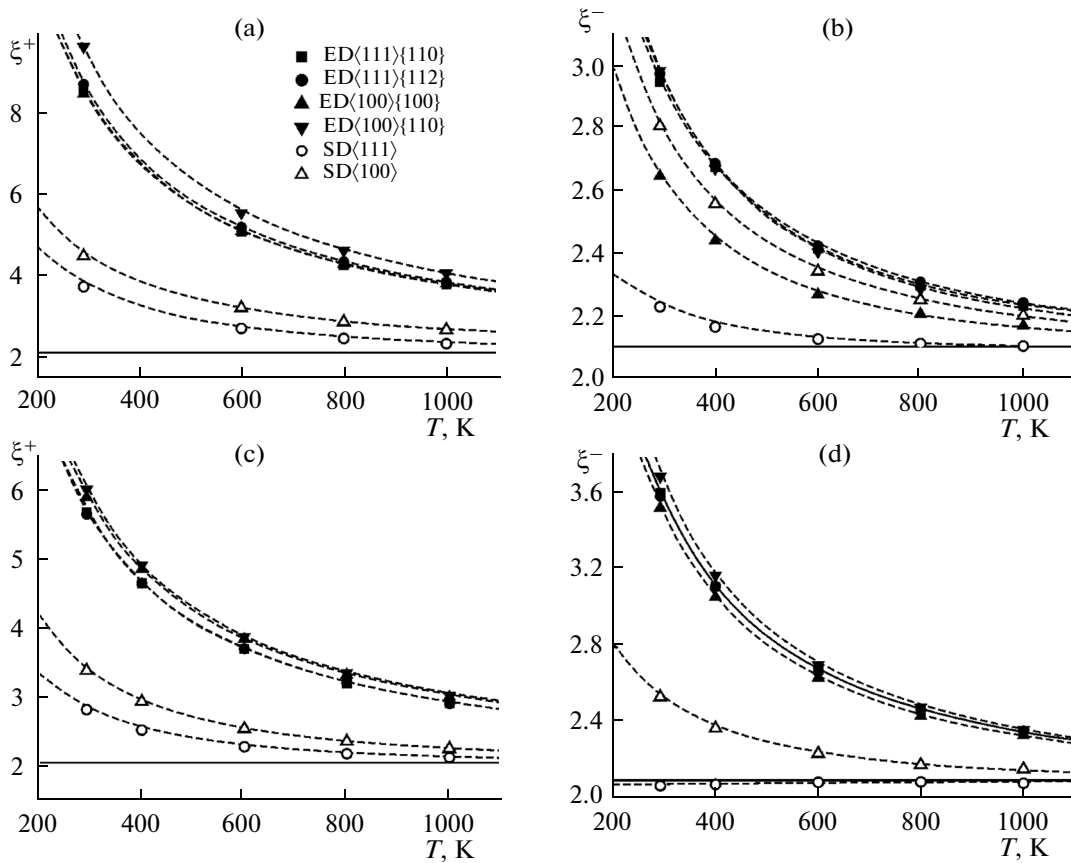| Dislocations	A^+ (Fe; V)	B^+ (Fe; V)	A^- (Fe; V)	B^- (Fe; V)
ED$\langle 111 \rangle \{110\}$	942; 551	6148; 3680	154; 265	1116; 1232
ED$\langle 111 \rangle \{112\}$	966; 548	6508; 3719	157; 260	1133; 1275
ED$\langle 100 \rangle \{100\}$	927; 573	7311; 4828	113; 254	719; 1169
ED$\langle 100 \rangle \{110\}$	1105; 593	5949; 4689	168; 281	932; 1230
SD$\langle 111 \rangle$	300; 162	1185; 774	34; −11	504; 170
SD$\langle 100 \rangle$	366; 245	3521; 1082	135; 89	900; 727

Fig. 3. Temperature dependences of the dislocation sink efficiency in Fe and V BCC crystals with the dislocation density of $3 \times 10^{14} \, \text{m}^{-2}$ for various types of dislocations (shown in figure) for (a) Fe and SIA; (b) Fe and vacancy; (c) V and SIA; (d) V and vacancy. The solid lines are the NILS efficiencies. The dotted lines are dependence (9) with the values of parameters A and B from Table 3.
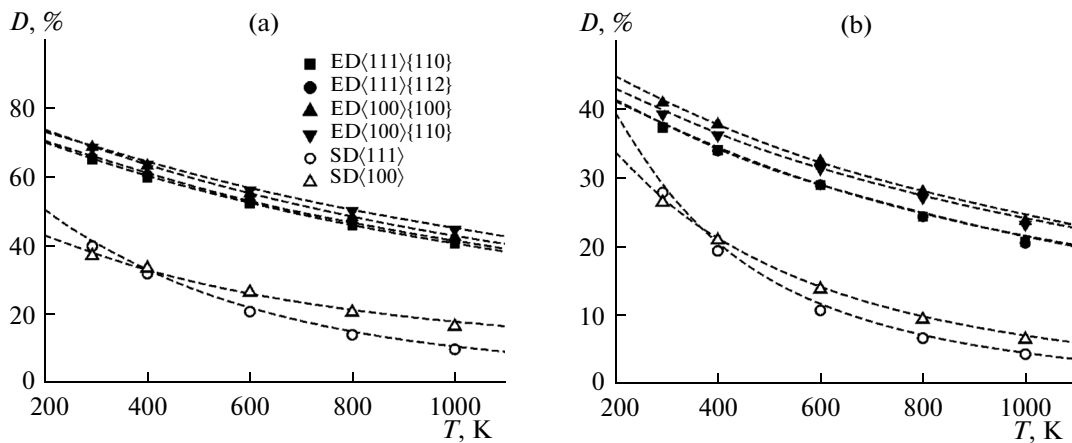

Fig. 4. Temperature dependences of the dislocation bias factor D in Fe and V BCC crystals with the dislocation density of $3 \times 10^{14} \, \text{m}^{-2}$ for various types of dislocations (shown in figure): (a) Fe; (b) V. The dotted lines are plotted with the use of (9) and data from Table 3.

culated for ED⟨110⟩{110}, ED⟨100⟩{100}, and SD⟨111⟩ dislocations at $T = 293$ K in the model crystallites with sizes L (in the lattice parameters a) of 200, 240, 300, 400, 600, 1000, and 3000, which corresponds to the values of ρ_d (in $10^{13} \, \text{m}^{-2}$) of 30, 21, 14,

7.6, 3.4, 1.2, and 0.14 in Fe and 27, 19, 12, 6.9, 3.0, 1.1, and 0.12 in V.

The OKMC (Fig. 5) data obtained over the considered dislocation density range are well described by the dependence
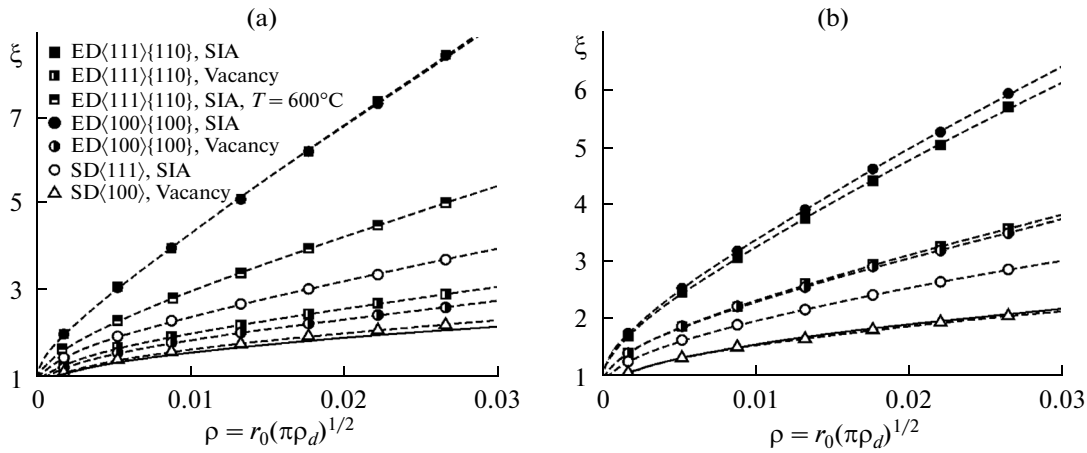
Fig. 5. DS efficiency ξ as a function of parameter $\rho = r_0(\pi\rho_d)^{1/2}$ at 293 K (if no other temperature is indicated in figure) in BCC crystals: (a) Fe, (b) V. The solid lines are dependences (8) for the NILS efficiencies. The dotted lines are approximations (10) of the calculated data.

$$\xi(\rho) = s\xi_0(\rho) + t\rho, \qquad (10)$$

where $\rho = r_0(\pi\rho_d)^{1/2}$ and $\xi_0(\rho)$ is determined by means of (8), and s and t are fitting parameters (Table 4).

The results of the analyzed relationship between the values of fitting parameters s and t are given in Appendix B.

It is seen from the data (Fig. 5) that taking into account the interaction of SPD with DS noticeably amplifies the impact of the dislocation density on the DS efficiency.

CONCLUSIONS

(i) In Fe and V BCC crystals, the DS efficiencies for SPDs (SIAs and vacancies) were calculated via the object kinetic Monte-Carlo method in the temperature range of 293–1000 K with the dislocation density values of $1 \times 10^{12} - 3 \times 10^{14}$ m^{-2}. The screw and edge dislocations with the $1/2\langle 111 \rangle$ and $\langle 100 \rangle$ Burgers vectors were considered in the $\langle 111 \rangle\{110\}$, $\langle 111 \rangle\{112\}$, $\langle 100 \rangle\{100\}$, and $\langle 100 \rangle\{110\}$ slip systems. The energies of elastic interaction of SPDs with dislocations were calculated within the anisotropic linear theory of elasticity, and the point defect characteristics (the parameters of elastic dipoles) at stable and metastable positions evaluated via molecular statistics [6, 16–18] were used. The linear sinks not interacting with SPDs and

possessing a certain SPD absorption radius at their diffusive migration in the crystal were studied as well. The direction, densities, and absorption radii of NILS correspond to the DS ones.

(ii) The dislocation sink efficiency for SPD depends weakly on the dislocation slip system at a given angle between dislocations and Burgers vector (in the limits of 12% at a temperature of 293 K).

(iii) All considered dislocations (edge and screw ones) are more effective sinks for SIAs than for vacancies. The differences in the dislocation sinks efficiencies for SIAs and vacancies decrease with the increase in temperature.

(iv) The dislocation sink efficiency was found to decrease with increasing temperature and to be defined by the equation

$$\xi(T) = \xi_0\left[1 + AT^{-1}\exp\left(-\frac{T}{B}\right)\right],$$

where A and B are fitting parameters (Table 3) and ξ_0 is the NILS efficiency.

(v) Taking into account elastic (field) interaction of SPDs with their dislocation sinks considerably amplified the impact of the dislocation density on the dislocation sink efficiency. The dislocation sink efficiency

Table 4. Values of parameters $s^{\pm}$ and $t^{\pm}$ ("+" for SIA and "−" for vacancies) in (10) for various types of dislocations in Fe and V BCC crystals with the dislocation density of 3×10^{14} m^{-2}

Dislocations	T, K	s^+ (Fe; V)	t^+ (Fe; V)	s^- (Fe; V)	t^- (Fe; V)
ED$\langle 111 \rangle\{110\}$	293	1.458; 1.429	204.0; 101.2	1.163; 1.255	18.44; 35.71
ED$\langle 111 \rangle\{110\}$	600	1.383; −	81.31; −	−; −	−; −
ED$\langle 100 \rangle\{100\}$	293	1.477; 1.458	200.8; 108.3	1.113; 1.254	11.33; 33.13
SD$\langle 111 \rangle$	293	1.273; 1.149	40.18; 17.45	1.027; 0.9965	2.586; −0.902

with the dislocation density $\rho_d < 3 \times 10^{14}$ m^{-2} is defined by the equation

$$\xi(\rho) = s\xi_0(\rho) + t\rho,$$

where $\rho = r_0(\pi\rho_d)^{1/2}$, $\xi_0(\rho)$ is determined from (8), and s and t are fitting parameters (Table 4).

ACKNOWLEDGMENTS

APPENDIX A

Solving the diffusion equation for NILS efficiency results in [23, 24]

$$\xi_{0,th}(\rho) = \frac{2\pi(1-\rho^2)}{\ln\left(\frac{1}{\rho}\right) - \frac{3}{4} + \frac{1}{4}\rho^2(4-\rho^2)}, \qquad (A.1)$$

where $\rho = r_0(\pi\rho_d)^{1/2}$.

Equation (A.1) was obtained for NILS which is a hollow cylinder. In the present work, we assume that the cylinder being a sink contains crystal atoms, and therefore, in the calculation of the DS and NILS efficiency, the possibility of formation of SPDs inside the cylinder was taken into account. In this case, SPD was assumed to be absorbed by a sink immediately after formation without any jump. Taking into account this fact requires the modification of the right part of equation (A.1), namely, multiplying by $(1 + \rho^2)$. In addition, since the maximum ρ used in this work takes the value of $0.015\pi^{1/2}$, the terms on the order of ρ^4 can be neglected. Thereby, (A.1) can be written as follows

$$\xi_{0,th}(\rho) = \frac{2\pi}{\ln\left(\frac{1}{\rho}\right) - \frac{3}{4} + \rho^2}. \qquad (A.2)$$

Expressions (A.1) and (A.2) do not take into account the finite length of SPDs jumps, which results in the dependence of the NILS efficiency not only on the value of ρ but also on the value of r_0 [16]. In addition, since the diffusive mechanisms for SIA and vacancy are different (the vacancy completes a jump to one of the eight nearest lattice sites, while the SIA does

so to one of the four nearest sites), the equations for a vacancy and SIA are expected to be different. In order to refine the expressions obtained in [16], we performed calculations of the NILS efficiency along the $\langle 100 \rangle$ direction for SPDs at various values of ρ_0 and r_0 via the OKMC method with increased accuracy (10^7 trajectories for each case). Analysis of the data enabled us to obtain the following dependences:

$$\xi_0^{\pm}(\rho, r_0) = \xi_a(\rho)$$
$$\times \left[1 - F\xi_a(\rho)\frac{l}{r_0}\left(1 - G\xi_a(\rho)\frac{l}{r_0} + H^{\pm}\frac{l}{r_0}\right)\right], \qquad (A.3)$$

where $F = 0.047$, $G = 0.066$, $H^+ = 0.41$, $H^- = 0.25$, and ξ_a is the asymptotic value of NILS efficiency when r_0/l tends to infinity.

The value of ξ_a is close to $\xi_{0,th}$ determined from (A.2), and with decreasing ρ, the difference between them decreases. The difference in these values is determined by using various boundary conditions in [23, 24] and in this work. The maximum difference in these values (at $\rho = 0.015\pi^{1/2}$) is ~0.4%. Numerical analysis of data revealed that the value of ξ_a is accurately described by the expression

$$\xi_a(\rho) = \xi_{0,th}(\rho)\{1 - 0.0011\xi_{0,th}(\rho)$$
$$\times [1 + 0.14\xi_{0,th}(\rho)(1 + 0.25\xi_{0,th}(\rho))]\}. \qquad (A.4)$$

The value of $\xi_0^{\pm}$ depends also on the NILS direction. The OKMC calculations revealed the maximum values of $\xi_0^{\pm}$ for NILSs oriented along the $\langle 100 \rangle$ direction and the minimum value for the $\langle 111 \rangle$ direction. Table A.1 shows the OKMC-calculated values of $\xi_0^{\pm}$ for NILS along various crystallographic directions at $r_0 = 3a$ and $\rho = 0.015\pi^{1/2}$.

APPENDIX B

Analysis of the correlation between fitting parameters A and B for all considered dislocation types, SPD, and materials (Table 3) revealed the following relation between them:

$$\frac{A}{B} \approx 0.15. \qquad (B.1)$$

Parameter B for a given DS type can thus be calculated from (9) and (B.1) for the known value of DC efficiency ξ_1 at $T = T_1$:

$$B = \frac{T_1}{W\left(\frac{0.15\xi_0}{|\xi_1 - \xi_0|}\right)}, \qquad (B.2)$$

where $W(x)$ is the Lambert function (inverse function to $f(w) = we^w$).

The dependences obtained with the use of (9), (B.1), and (B.2), where values of ξ at $T = 293$ K were

Table A.1. NILS efficiencies $\xi_0^{\pm}$ (ρ, r_0) ("+" for SIA and "−" for vacancies, $\rho = 0.015\pi^{1/2}$, $r_0 = 3a$) in accordance with various crystallographic directions in BCC crystals. The relative error is under 0.05%

$\xi_0^{\pm}$ (ρ, r_0)	NILS crystallographic direction			
	$\langle 100 \rangle$	$\langle 110 \rangle$	$\langle 111 \rangle$	$\langle 112 \rangle$
ξ_0^+	2.104	2.101	2.094	2.100
ξ_0^-	2.107	2.106	2.098	2.106

taken as ξ_1 (Table 2), describe the OKMC data well over the considered temperature range.

APPENDIX C

Analysis of the correlation between fitting parameters s and t for all considered dislocation types, SPD, and materials (Table 4) revealed that, if $\xi < 6$ at $\rho_d = 3 \times 10^{14}$ m^{-2}, then parameters s and t are related to each other by the empirical relation

$$t = 18\{\exp[4.2(s-1)] - 1\}. \qquad (C.1)$$

Thus, if the DS efficiency ξ_1 at $\rho = \rho_1$ $(\rho_d = \rho_{d,1})$ is known, then from (10) and (C.1) parameter t for the given DS type can be calculated as

$$t = -\frac{1}{4.2} W\left[4.2\frac{18\rho}{\xi_{0.1}}\exp\left(4.2\frac{\xi_1 - \xi_{0.1} + 18\rho}{\xi_{0.1}}\right)\right] \\ + \frac{\xi_1 + 18\rho}{\xi_{0.1}}, \qquad (C.2)$$

where $\xi_{0.1} = \xi_0(\rho_1)$.

The value of ξ^+ at $\rho_d = 3 \times 10^{14}$ m^{-2} is above 8 for the edge dislocations in Fe at $T = 293$ K. The fitting of their calculated dependences $\xi^+(\rho)$ by expression (10) gives 1.47 and 202 for parameters s and t, respectively (Table 4), which do not satisfy (C.1). Upon increasing T to 600 K, the value of ξ^+ for the dislocations at $\rho_d = 3 \times 10^{14}$ m^{-2} decreases to 5.1, and expressions (10), (C.1), and (C.2) successfully describe the OKMC data.

The obtained relations (10), (C.1), and (C.2) make it possible to calculate the DS efficiency for any value of ρ_d from the considered range at a known value of this efficiency for any other value of ρ_d.

REFERENCES

1. Johnson, R.A. and Orlov, A.N., *Physics of Radiation Effects in Crystals*, Amsterdam: Elsevier, 1986.
2. Indenbom, V.L. and Lothe, J., *Elastic Strain Fields and Dislocation Mobility*, Amsterdam: Elsevier, 1992.
3. Slezov, V.V., Subbotin, A.V., and Osmayev, O.A., Evolution of a microstructure of materials under irradiation, *Phys. Solid State*, 2005, vol. 47, pp. 477−483.
4. Voyevodin, V.N. and Neklyudov, I.M., *Evolyutsiya strukturnofazovogo sostoyaniya i radiatsionnaya stoykost' konstruktsionnykh materialov* (Evolution of Structure and Phase State and Radiation Resistance of Structural Materials) Kiev: Naukova Dumka, 2006.
5. Kröner, E., Allgemeine Kontinuumstheorie der Versetzungen und Eigenspannungen, *Arch. Rat. Mech. Anal.*, 1959/60, vol. 4, pp. 273−334.
6. Sivak, A.B., Chernov, V.M., Dubasova, N.A., and Romanov, V.A., Anisotropy migration of self-point defects in dislocation stress fields in bcc Fe and fcc Cu, *J. Nucl. Mater.*, 2007, vol. 367−370, pp. 316−321.
7. Sivak, A.B., Chernov, V.M., and Romanov, V.A., Diffusion of self-point defects in body-centered cubic iron crystal containing dislocations, *Crystallogr. Rep.*, 2010, vol. 55, no. 1, pp. 97−108.
8. Brailsford, A.D., Bullough, R., and Hayns, M.R., Point defect sink strengths and void-swelling, *J. Nucl. Mater*, 1976, vol. 60, pp. 246−256.
9. Wolfer, W.G., The dislocation bias, *J. Computer-Aided Mater. Des.*, 2007, vol. 14, pp. 403−417.
10. Caturla, M.J., Soneda, N., Alonso, E., Wirth, B.D., Diaz de la Rubia, T., and Perlado, J.M., Comparative study of radiation damage accumulation in Cu and Fe, *J. Nucl. Mater,* 2000, vol. 276, nos. 1−3, pp. 13−21.
11. Caturla, M.J., Soneda, N., Diaz de la Rubia, T., and Fluss, M., Kinetic Monte Carlo simulations applied to irradiated materials: The effect of cascade damage in defect nucleation and growth, *J. Nucl. Mater.,* 2006, vol. 351, pp. 78−87.
12. Stoller, R.E., Golubov, S.I., Domain, C., and Becquart, C.S., Mean field rate theory and object kinetic Monte Carlo: A comparison of kinetic models, *J. Nucl. Mater.*, 2008, vol. 382, pp. 77−90.
13. Hirth, J.P. and Lothe, J., *Theory of Dislocations,* New York: Wiley, 1982.
14. Domain, C., Becquart, C.S., and Malerba, L., Simulation of radiation damage in Fe alloys: An object kinetic Monte Carlo approach, *J. Nucl. Mater.*, 2004, vol. 335, pp. 121−145.
15. Caturla, M.J., Diaz de la Rubia, T., and Fluss, M., Modeling microstructure evolution of f.c.c. metals under irradiation in the presence of He, *J. Nucl. Mater.,* 2003, vol. 323, pp. 163−168.
16. Sivak, A.B., Chernov, V.M., Romanov, V.A., and Sivak, P.A., Kinetic Monte-Carlo simulation of self-point defect diffusion in dislocation elastic fields in bcc iron and vanadium, *J. Nucl. Mater.,* 2011, vol. 417, pp. 1067−1070.
17. Romanov, V.A., Sivak, A.B., and Chernov, V.M., Crystallographic, energetic and kinetic properties of self-point defects and their clusters in BCC iron. 1. Semiempirical model of BCC iron and potential of interatomic interaction, *Vopr. At. Nauki Tekhn., Ser. Materialoved. Nov. Mater.*, 2006, vol. 66, pp. 129−150.
18. Romanov, V.A., Sivak, A.B., Sivak, P.A., and Chernov, V.M., Equilibrium and diffusion characteristics of self-point defects in vanadium, *Vopr. At. Nauki Tekhn. Ser. Termoyad. Sintez*, 2012, no. 2, pp. 60−80.
19. Indenbom, V.L. and Chernov, V.M., Thermally activated glide of a dislocation in a point defect field, in Indenbom, V.L. and Lothe, J., *Elastic Strain Fields and Dislocation Mobility,* Amsterdam: Elsevier, 1992, pp. 570.
20. Teodosiu, C., *Elastic Models of Crystal Defects,* Berlin: Springer-Verlag, 1982.
21. Leibfried, G. and Breuer, N., *Point Defects in Metals. I: Introduction to the Theory*, Berlin: Springer-Verlag, 1978.
22. Zinovyev, V.E., *Teplofizicheskiye svoystva metallov pri vysokikh temperaturakh* (Heat-Physical Properties of Metals under High Temperatures), Moscow: Metallurgiya, 1989.
23. Wiedersich, W., On the theory of void formation during irradiation, *Radiation Effects*, 1972, vol. 12, pp. 111−125.
24. Nichols, F.A., On the estimation of sink-absorption terms in reaction-rate-theory analysis of radiation damage, *J. Nucl. Mater.,* 1978, vol. 75, pp. 32−41.

Translated by O. Maslova